Article

A Comparative Study on Satellite- and Model-Based Crop Phenology in West Africa

Elodie Vintrou [1,*]**, Agnès Bégué** [1]**, Christian Baron** [1]**, Alexandre Saad** [1]**, Danny Lo Seen** [1] **and Seydou B. Traoré** [2]

[1] CIRAD UMR TETIS, Maison de la Télédétection, 500 rue J.F. Breton, Montpellier, France;
E-Mails: agnes.begue@cirad.fr (A.B.); christian.baron@cirad.fr (C.B.);
alexandre.saad@cirad.fr (A.S.); loseen@cirad.fr (D.L.S.)

[2] Centre Régional AGRHYMET, 0425 Bld de l'Université, BP 11 011 Niamey, Niger;
E-Mail: s.traore@agrhymet.ne

* Author to whom correspondence should be addressed; E-Mail: elodie.vintrou@cirad.fr;
Tel.: +33-467-548-754.

Abstract: Crop phenology is essential for evaluating crop production in the food insecure regions of West Africa. The aim of the paper is to study whether satellite observation of plant phenology are consistent with ground knowledge of crop cycles as expressed in agro-simulations. We used phenological variables from a MODIS Land Cover Dynamics (MCD12Q2) product and examined whether they reproduced the spatio-temporal variability of crop phenological stages in Southern Mali. Furthermore, a validated cereal crop growth model for this region, SARRA-H (System for Regional Analysis of Agro-Climatic Risks), provided precise agronomic information. Remotely-sensed green-up, maturity, senescence and dormancy MODIS dates were extracted for areas previously identified as crops and were compared with simulated leaf area indices (LAI) temporal profiles generated using the SARRA-H crop model, which considered the main cropping practices. We studied both spatial (eight sites throughout South Mali during 2007) and temporal (two sites from 2002 to 2008) differences between simulated crop cycles and determined how the differences were indicated in satellite-derived phenometrics. The spatial comparison of the phenological indicator observations and simulations showed mainly that (i) the satellite-derived start-of-season (SOS) was detected approximately 30 days before the model-derived SOS; and (ii) the satellite-derived end-of-season (EOS) was typically detected 40 days after the model-derived EOS.

Studying the inter-annual difference, we verified that the mean bias was globally consistent for different climatic conditions. Therefore, the land cover dynamics derived from the MODIS time series can reproduce the spatial and temporal variability of different start-of-season and end-of-season crop species. In particular, we recommend simultaneously using start-of-season phenometrics with crop models for yield forecasting to complement commonly used climate data and provide a better estimate of vegetation phenological changes that integrate rainfall variability, land cover diversity, and the main farmer practices.

Keywords: phenology; crops; MODIS; SARRA-H model; practices; Mali

1. Introduction

Crop phenological dynamics should be essential for evaluating crop production [1], especially in the West African food-insecure regions. Vegetation conditions must be carefully monitored using early warning systems during the critical growth stages when estimating year-end crop yields in these regions. There, millet and sorghum, like other cereals, are cultivated under rainfed conditions. Thus, the timing of the photoperiodic phenological stages for these crops varies from year to year due to variable sowing dates, which are farm-level management decisions that depend on soil moisture and temperature conditions following the onset of rainfall [2].

Over the last two decades, global remote sensing dataset availability has provided new means for studying global vegetation patterns and dynamics [3,4]. With the ability to detect surface phenology objectively on a uniform timescale and global scale, time series composed of low- and medium-resolution satellite images have been used to study the phenological patterns that relate to climate variability and human actions (e.g., [5–9]). A variety of methods has been developed to detect vegetation phenology timing from satellite time series. White *et al.* [10], Schwartz and Hanes [11], and Hmimina *et al.* [12] reviewed these methods, and Atkinson *et al.* [13] discussed the very large differences one finds when using different phonological extraction techniques. For example, start-of-season vegetation may be derived from the seasonal NDVI curve [14–16] or precipitation data characteristics [17–19]. As vegetation phenology in arid and semiarid ecosystems is primarily controlled by water availability, a number of field studies have attempted to quantitatively link phenology to precipitation forcing. For example, Zhang *et al.* [3] examined how phenology changed with latitude, and how it was related to the timing of seasonal rainfall in Sahelian and Sudanese regions; they concluded that well-defined thresholds exist in cumulative rainfall for stimulating vegetation green-up in arid and semiarid regions of Africa.

However, where weather stations are sparse and data access is difficult, climatic data are either aggregated, extrapolated from weather stations, or estimated from low spatial resolution satellite data [20]. To run agro-meteorological models, GCM or satellite-derived rainfall data are not satisfactory due to aggregation issues [21,22]. Using interpolated ground data, the model output uncertainty can be high where rainfall displays strong spatial variability because agricultural production is also sensitive to rainfall levels and temporal distribution. Moreover, on a regional scale,

vegetation phenology also depends on soil, micro-climates, regional climates, land use and management, for which complex spatio-temporal phenology patterns can be observed [23]. Thus, remotely sensed vegetation index (VI) data should include the main intra-seasonal vegetation dynamics and integrate both rainfall variability and land cover status. This is the reason why without field observations on a large scale, satellite-derived phenological indicators could be relevant for food security early warning systems, which may indicate risky situations in the region due to delayed crop growth.

In this study, the objectives were to (i) qualify MODIS MCD12Q2 product, which increasingly interest the agricultural community and should grow in the future to monitor crops on a regional or global scale and (ii) test whether phenology variables (phenometrics) derived from a MODIS Land Cover Dynamics Yearly (MCD12Q2) product express the spatio-temporal variability of crop phenological stages in Southern Mali. The few ground phenology and/or cropping practice observations on the local scale for several years prohibits data validation from the ground and a deeper analysis of the phenology. However, a validated crop growth model for the sub-Saharan regions (SARRA-H, System for Regional Analysis of Agro-Climatic Risks) [24] provides precise agronomic information, which was well-documented using local varieties that are mainly cultivated by farmers in this area [24–26]. The model can reproduce the evolution of phenological stages and leaf area indices (LAI) of different tropical cereal species and varieties with mainly rainfall, temperature, global radiation, and evapotranspiration as input data. However, this model requires local information, such as the main practices (e.g., species, varieties, intense or extensive practices, and early sowing date strategies), and must be forced using climate data that are relevant on a local scale.

Thus, the methodology consisted in examining whether the satellite observations and crop phenology agro-simulations are consistent. Phenometrics derived from the MODIS time series were compared to crop model simulations for sites throughout South Mali and located near synoptic stations with available rainfall and climatic data. Both the spatial (north-south gradient) and temporal (inter-annual) differences between the satellite- and model-derived phenological indicators were analyzed; we conclude on the potential for combining satellite- and model-derived indicators of crop phenology to improve agricultural production estimates on a national scale in West Africa.

2. Material

2.1. Study Area

Mali is a land-locked West African country between the latitudes 10 °N and 24 °N (Figure 1 [27]). Mali exhibits a latitudinal climatic gradient that ranges from sub-humid to semi-arid and extends further north to arid and desert regions. Similar to other West African countries along the same latitudinal belt, food security requires adequate rainfall during the cropping season. Farming is the main source of income for many people in this region; rainfed millet and sorghum are the major food crops. The vast majority of the population (80%) includes subsistence farmers. A few larger farms produce crops for sale (cash crops), mainly cotton and peanuts. In this study, we do not consider the Saharan zone in the northern areas of the country with sparse rainfall of less than 300 mm per year.

- Food-producing agriculture: area dedicated to millet and sorghum (>50%) as well as cotton (<10%);

- Intensive agriculture: area dedicated to maize and cotton (>40%);
- Mixed agriculture: area dedicated to sorghum (>20%) and cotton (between 5% and 40%).

Figure 1. The synoptic station locations and a map of the crop production systems in South Mali [27].
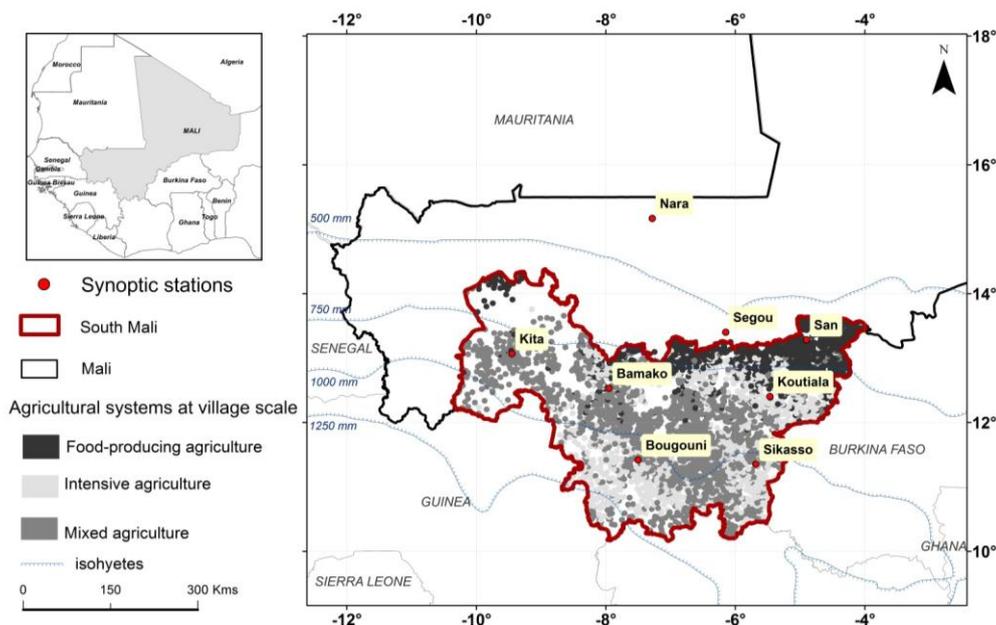

2.2. Satellite Data

2.2.1. The MODIS Land Cover Dynamics Product (MCD12Q2)

Two MCD12Q2 tiles that cover Mali were downloaded for 2002 to 2008. The yearly MODIS Land Cover Dynamics product (MCD12Q2; [28]) was developed to support seasonal phenology and inter-annual variation studies on land surface and ecosystem properties. The Collection 5 land cover dynamics product is described in Ganguly *et al.* [29] and available online for 2000 to 2010 (accessible from [30]) at a 500-m spatial resolution. This product was generated each year using the eight-day vegetation index EVI (Enhanced Vegetation Index) calculated from the NBAR reflectance (Nadir Bidirectional Reflectance Distribution Function—Adjusted Reflectance). Two full years of NBAR EVI observations were assembled using a window with six months of data before and after the 12-month period of interest. The EVI was used because it provides a greater dynamic range than the normalized difference vegetation index [31].

The Land Cover Dynamic product is based on Zhang *et al.*'s [23] algorithm that models the annual vegetation index increase and decrease through a series of logistic functions developed using 24 months of input data (*i.e.*, data for the 12 months of interest bracketed by six months of earlier and later data). This algorithm, also used in Beck *et al.* [32], characterizes vegetation growth cycles using four transition dates based on the EVI curvature-change rate from the MODIS data time series: (1) green-up: the date of onset for the EVI increase, typically referred to as start-of-season (SOS); (2) maturity: the date of onset for the EVI maximum, typically referred to as start-of-maximum (SMAX); (3) senescence: the date of onset for the EVI decrease, typically referred to as end-of-maximum (EMAX); and (4) dormancy: the date of onset for the EVI minimum, typically

referred to as end-of-season (EOS) [29] (Figure 2). Each variable is encoded on two distinct layers (*n* and *n* + 1) to include two growing seasons per year.

Figure 2. Four transition dates based on the EVI curvature-change rate from the MODIS data time series. The solid line is an ideal time series for the vegetation index data, and the dashed line is the rate of change in the VI data curvature. The circles indicate transition dates: 1: start-of-season (SOS); 2: start-of-maximum (SMAX); 3: end-of-maximum (EMAX); and 4: end-of-season (EOS), adapted from Figure 2 in [23].
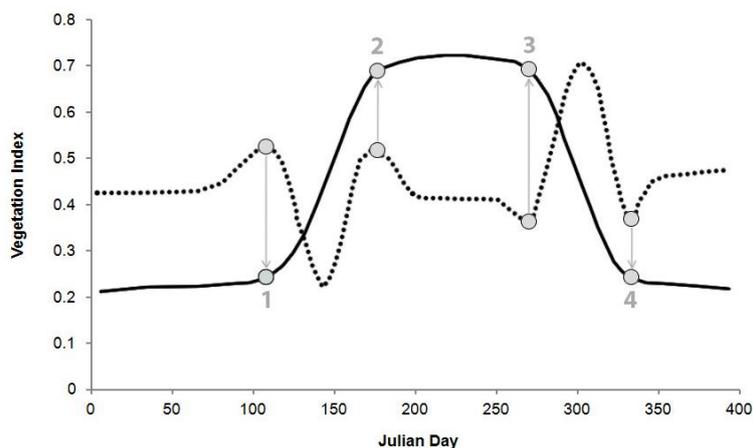
2.2.2. MCD12Q2 Product Pre-Processing

Previous studies showed that the MODIS MCD12Q2 product displayed inconsistencies in certain pixel values [33,34]. For the Southern Mali images, Vintrou *et al.* [34] showed that only 70% of the cropped pixels had complete phenology information on the full vegetation cycle (four phenometrics values), and a large part of the pixels displayed unrealistically late start-of-season (SOS) values. The SOS frequency histogram displayed two peaks of high frequency, and Vintrou *et al.* [34] showed that the second peak was due to data gaps in the increasing part of the EVI time profiles, that conducted to a bad fit of Zhang's model. To eliminate these outliers, we modeled the SOS value distribution using two Gaussian functions and removed the pixels that corresponded to the second peak.

2.3. Cropland and Agricultural System Maps

A cultivated domain map for Mali (2 classes: "crop" and "non-crop") was produced at a 250-m spatial resolution by Vintrou *et al.* [35] using the 2007 MODIS time series.

A map of the agricultural systems was also produced for South Mali using spectral, spatial, temporal and textural indicators extracted from the 2007 MODIS images combined with ground data [27]. For this map, each of the 4,000 villages in the studied area were assigned to one of the three agricultural system classes, as shown in Figure 1. The food-producing agriculture class corresponds to villages with agricultural area with millet and sorghum (>50%) as well as cotton (<10%). Villages with an intensive agricultural system essentially grow maize and cotton (>40%), and the mixed agriculture class corresponds to agricultural area with both sorghum (>20%) and cotton (between 5% and 40%).

2.4. Climate Data

The Agro-Hydro-Meteo Regional Center (AGRHYMET) provided daily climatic data (rainfall, temperature, and insolation) from eight synoptic stations in Mali for 2007 (Table 1). For two stations among the eight, one in Sahelian (Segou) and the other in the Sudano-Guinean zone (Sikasso), the data covered the seven-year period between 2002 and 2008 (Table 2).

Table 1. Synoptic station characteristics from north to south.

Station	Latitude (dd)	Longitude (dd)	2007 Rainfall (mm)	Cropping System
Nara	15.17	−7.29	441	Food-producing agriculture
Segou	13.4	−6.16	521	Food-producing agriculture
San	13.29	−4.91	748	Food-producing agriculture
Kita	13.07	−9.46	883	Mixed agriculture
Bamako	12.53	−7.95	856	Mixed agriculture
Koutiala	12.4	−5.47	962	Intensive agriculture
Bougouni	11.41	−7.51	1,330	Mixed agriculture
Sikasso	11.35	−5.69	1,357	Intensive agriculture

Table 2. Segou and Sikasso annual rainfall (mm) from 2002 to 2008.

Year	Segou	Sikasso
2002	500	780
2003	610	1,160
2004	500	1,140
2005	480	1,010
2006	560	970
2007	520	1,360
2008	680	950

2.5. The SARRA-H Crop Model

SARRA-H (System for Regional Analysis of Agro-Climatic Risks) is a simple, deterministic crop model for cereals that operates using daily time steps and was implemented on the Ecotrop platform of the Centre International de Recherche Agronomique pour le Développement (CIRAD) [36–38]. This platform facilitates managing different models (versions), data and simulation scenarios. The model used herein was SARRA-H version 3.2 to simulate the biomass dynamics (root, stem, leaves, and grains), especially in several select millet, maize, and sorghum varieties. The model reproduces three major processes: evolution of the phenological stages for the varieties (cycle length and photoperiodism) and carbon (biomass and distribution changes) and water balance [36]. The simulated biomass production is constrained by the availability of two main resources: light energy and soil water; AGRHYMET is currently adapting its crop yield forecasting system to provide information on productivity for different crops, crop varieties or intensification levels.

The model uses daily climate data (rainfall, global radiation or insolation, temperature, and evapotranspiration), soil type, agricultural practices information, and crop variety. Furthermore, a number of empirical constants were used for the soil moisture and crop state criteria to initiate

sowing, the automatic test modalities during the seedling stage for stress-induced crop failure, and the automatic replanting option in case of failure [39]. Depending on whether the crop is traditional (photo-period sensitive) or improved (insensitive), it will mature either on a relatively stable calendar date or after a genotype-specific growth duration [40]. During that period, the crop will undergo variable levels of drought with variable effects on crop growth dynamics and yield as the phenological phases change with stress sensitivity [25,41].

3. Methods

3.1. Satellite-Derived Phenometrics

A 250-m resolution map of the cultivated domain was used to select the 500-m resolution MODIS MCD12Q2 pixels with a high proportion of crops covered. We used a two-stage filter ensure the selection of pure crop pixels phenology. We first applied a 3×3 sum filter to the 250-m crop mask and retained the pixels with a score greater or equal to 7 (out of 9). The crop mask spatial resolution remained unchanged (250 m), but the crop pixels surrounded by non-crop pixels were not rejected from the phenology study. This was our "filtered crop mask". Second, to facilitate a high proportion of crops at a 500-m resolution, we applied the crop mask to the MODIS MCD12Q2 product with a majority filter (one pixel MODIS MCD12Q2 corresponds to four pixels of the crop mask) and kept the pure crop pixels only. The product is, hereafter, referred to as the crop phenology product (Figure 3).

We calculated the summary statistics (median and standard deviation) for the four phenometrics (SOS, SMAX, EMAX, and EOS) of the crop phenology product for a 10 km $\times$ 10 km window centered on each synoptic station.

Figure 3. An example of start-of-season extraction on a national scale (averaged on a 20 $\times$ 20 km grid) and Bougouni- and Segou-station scale (defined by a 10 $\times$ 10 km polygon) and masked using a 2007 crop map [35].
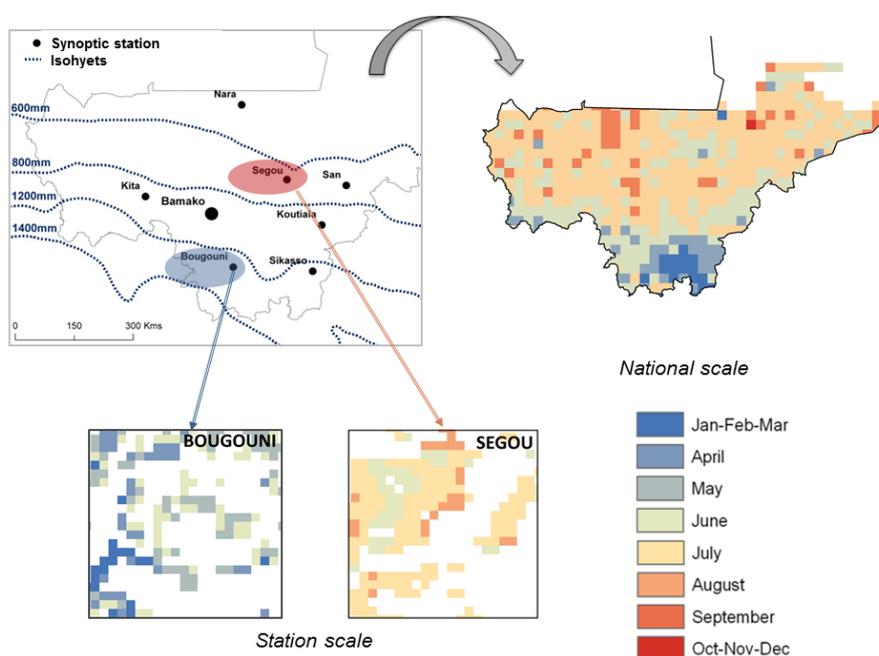
3.2. Model-Derived Phenometrics

3.2.1. Model Simulation Set

The SARRA-H model was used to predict crop behavior in their original environment (soil type) as a function of rainfall regimes and agricultural practices (crop species and variety, fertilization index, and sowing dates). For each synoptic station, we conducted 370 simulations using parameters from data in previous studies and expert knowledge (Table 3):

Table 3. System for Regional Analysis of Agro-Climatic Risks (SARRA-H) simulation input for each synoptic station.

Station	Species and Variety	Sowing Date	Fertilization	Soil Type	Soil Depth	Number of Simulations
Nara	Sorghum caudatum Millet souna	Intermediate	No	Sandy and sandy clay	80 cm and 180 cm	8
Segou	Sorghum guinea Sorghum kenikeba Millet choho	Late and intermediate	No	Sandy and sandy clay	80 cm and 180 cm	24
San	Sorghum guinea Sorghum kenikeba Millet choho	Late and intermediate	No	Sandy and sandy clay	80 cm and 180 cm	24
Kita	Sorghum guinea Sorghum kenikeba Millet choho Maize	Intermediate for millet and sorghum, and intermediate and late for maize	Yes/No	Sandy and sandy clay	80 cm and 180 cm	42
Bamako	Sorghum guinea Sorghum kenikeba Millet choho Maize	Late, intermediate	Yes/No	Sandy and sandy clay	80 cm and 180 cm	64
Koutiala	Sorghum guinea Millet choho Maize	Late and intermediate	Yes	Sandy and sandy clay	80 cm and 180 cm	32
Bougouni	Sorghum guinea Sorghum kenikeba Millet choho Maize	Early, late, intermediate (except for maize: intermediate and late only)	Yes/No	Sandy and sandy clay	80 cm and 180 cm	88
Sikasso	Sorghum guinea Sorghum kenikeba Millet choho Maize	Early, late, intermediate for millet and sorghum, and intermediate and late for maize	Yes/No	Sandy and sandy clay	80 cm and 180 cm	88

- Species composition and intensification mode: the species and intensification options were derived from the crop production systems map (Figure 1); the intensive and auto-subsistence

food-producing system crops were simulated using higher and lower fertilization levels, respectively.

- Species variety: the variety used was based on previous studies and expert knowledge; it mainly depends on the cropping season length and sowing strategies. Early and intermediate sowing dates imply photoperiodic varieties, and species adapted to the end of the rainy season were necessary; thus, we used photoperiodic (sorghum and pearl millet) and non-photoperiodic varieties (sorghum and maize).

- Soil type: soils in this region are mainly sandy [42]. The soil layer available for the rooting zone mainly depends on topography; it may be absent or may vary up to more than 2 m thick. Two types of soils (sandy and sandy clay) and two maximum root depths (80 cm and 180 cm) were examined to include the variability.

- Sowing date: the model automatically generated a sowing date that was the day when the available soil water was greater than 10 mm at the end of the day followed by a 20-day period, during which we monitored crop establishment [39]. If the daily simulated total biomass decreases 11 out of 20 days, the juvenile stage of the crop is considered a failure, which triggers automatic re-sowing. While the beginning of the growth cycle depends on the crop species, the sowing strategy is decided at the plot management level and considers the available labor and rainfall hazards. We use the most common strategy, wherein the end of the crop cycle (EOS) coincides with the end of the rainy season. Local photoperiodic millet and sorghum varieties were sown either as soon as the first rains began or later, depending on the growing season length. However, for maize and non-photoperiodic sorghum, the sowing dates depend on cycle length and the date the season typically ends, which varies from north to south.

Thus, in addition to rainfall parameters, the beginning of the crop cycle is based on previous studies [24,39] for pearl millet in Niger and sorghum in Mali [43]. For pearl millet and sorghum, the simulation starting dates were 1 March (to simulate early sowing), 1 May (to simulate intermediate sowing), and 1 July (to simulate late sowing). For maize, the simulation starting dates were, respectively, mid-June, 1 July, and mid-July. On average, and related to the beginning of the rainy season, the windows for the probable sowing dates also vary from north to south.

3.2.2. Model-Derived Phenometric Calculations

The four phenometrics of interest were derived from annual, temporal, LAI-simulated profiles using a daily time step for each station using the SARRA-H model (Table 3). The phenometrics calculations based on Zhang *et al.*'s [23] algorithm, using the R software version 2.9.1, were computed for each simulation of each station (e.g., 88 different SOS dates for Sikasso and Bougouni in 2007; Table 3) and the median was calculated for each phenometric, to generate a unique SOS, SMAX, EMAX, and EOS value for each synoptic station. The standard deviations were also calculated for each iteration to assess variability. The model sensitivity to varying soil types and fertilization modes was tested simultaneously.

3.3. Comparison between Satellite and Model-Derived Phenometrics

The satellite and model-derived phenometrics (median values for SOS, SMAX, EMAX, and EOS) were compared for each synoptic station/year combination by calculating the mean signed difference (MSD; Equation (1)) and the root mean square error (RMSE; Equation (2)), which is reported in days.

$$MSD = \frac{1}{N} \sum_{i=1}^{N} (M_i - O_i) \tag{1}$$

$$RMSE = \sqrt{\frac{1}{N} \sum_{i=1}^{N} (P_i - O_i)^2} \tag{2}$$

where O_i is the satellite-derived phenometrics, M_i is the model-derived phenometric, P_i is the predicted phenometric, and N is the number of points (number of stations or years, for the spatial and temporal analysis respectively). The RMSE is a frequently used measure of the differences between values predicted by a model and the values actually observed. In our case, we considered that the predicted values were obtained from a "statistical model", derived from the regression between model-derived and satellite-derived phenometrics (corresponding to the "ideal value" when the satellite and model fit perfectly).

4. Results

4.1. LAI Simulation Results

The LAI profiles simulated for each synoptic station as the annual SARRA-H crop model output exhibit a typical vegetation growth shape, except at the end of the growing season, where the LAI profile drops sharply (Figure 4).

Analyzing the model sensitivity to various soil types, fertilization modes and species composition, we observed the following:

- The choice of different soil types has a limited impact on LAI dynamics, except for EMAX (Table 4). For SOS, SMAX, and EOS, the soil effect was insignificant (bias < 5 days, except for Sikasso). For EMAX, the standard deviation between the different phenometrics using different types of soils varied from four to 12 days.
- The phenological indicators for fertilized crops appeared approximately five days earlier than for non-fertilized crops (Table 4). As an illustration, Figure 4 shows four LAI profiles for the Kita synoptic station in 2007 (one maize variety and one sorghum variety with two fertilizer treatments each).

A detailed analysis of the simulation results indicates that the main drivers of crop dynamics were species composition, planting strategies (early, intermediate, and late) and rainfall regime.

Figure 4. Examples of model-derived phenometrics (dotted lines) calculated with Zhang's non-linear functions for two sets of LAI simulations using the SARRA-H crop model for the Kita synoptic station in 2007. The green curve represents the maize LAI simulation (fertilized in the dark, non-fertilized in light); the orange curve represents the Guinea Sorghum LAI simulation (fertilized in the dark, non-fertilized in light). For each fertilized curve, the dotted lines correspond to the following from left to right: (i) start-of-season (SOS); (ii) start-of-maximum (SMAX) of season; (iii) end-of-maximum (EMAX) of season; and (iv) end-of-season (EOS).
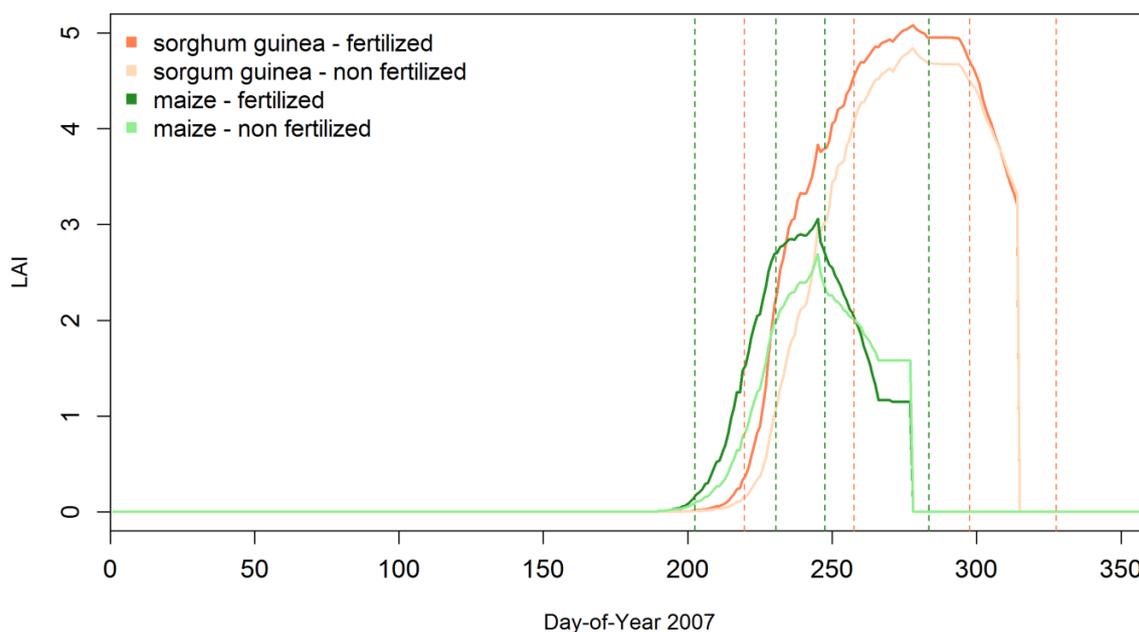

Table 4. The effect of soil type and fertilization mode on crop growth: standard deviations for the start-of-season, start-of-maximum of season, end-of-maximum of season, and end-of-season in days for each station, in 2007, with four soil types and two fertilization modes.

| Standard Deviation (days)	Nara	Segou	San	Kita	Bamako	Koutiala	Bougouni	Sikasso
Soil type factor:								
SOS	0	1	1	1	1	0	2	**10**
SMAX	1	1	1	3	3	0	3	6
EMAX	7	**12**	**10**	9	6	4	7	7
EOS	2	1	4	2	1	1	3	3
Fertilization mode:								
SOS				4	2		5	4
SMAX				5	7		**10**	5
EMAX				6	3		0	2
EOS				3	2		1	2

4.2. Phenometrics Spatial Analysis

4.2.1. North-South Gradient Analysis

Figure 5 shows the four MCD12Q2 product phenometrics calculated for each synoptic station in 2007. The north-south gradient for the start-of-season (SOS) metric was confirmed with a growing season that began in April in Sikasso, May in Bougouni, the end of June in Koutiala and Bamako, and the first half of July in San, Segou, and Kita, except for Nara, wherein the season began surprisingly earlier (27 June). The start-of-maximum (SMAX) was concentrated in the second half of August, while the end-of-maximum (EMAX) was concentrated in the second half of September, and the end-of-season occurred between mid-November and mid-December.

The four model-derived phenometrics calculated for each synoptic station, in 2007 (Figure 5), also confirm the SOS metric north-south gradient with a growing season that began in late June for Bougouni and Sikasso and the end of July-beginning of August for the other stations. The SMAX was concentrated in August, the EMAX was concentrated in October, and the end-of-season mainly occurred during the first half of November.

Figure 5. Satellite- (pink) and model-derived (violet) phenometrics boxplots were calculated for eight synoptic stations, ranged from north (**Top**) to south (**Bottom**), in 2007. The mean signed difference (MSD) is the difference between the model- and satellite-derived phenometric values in days.
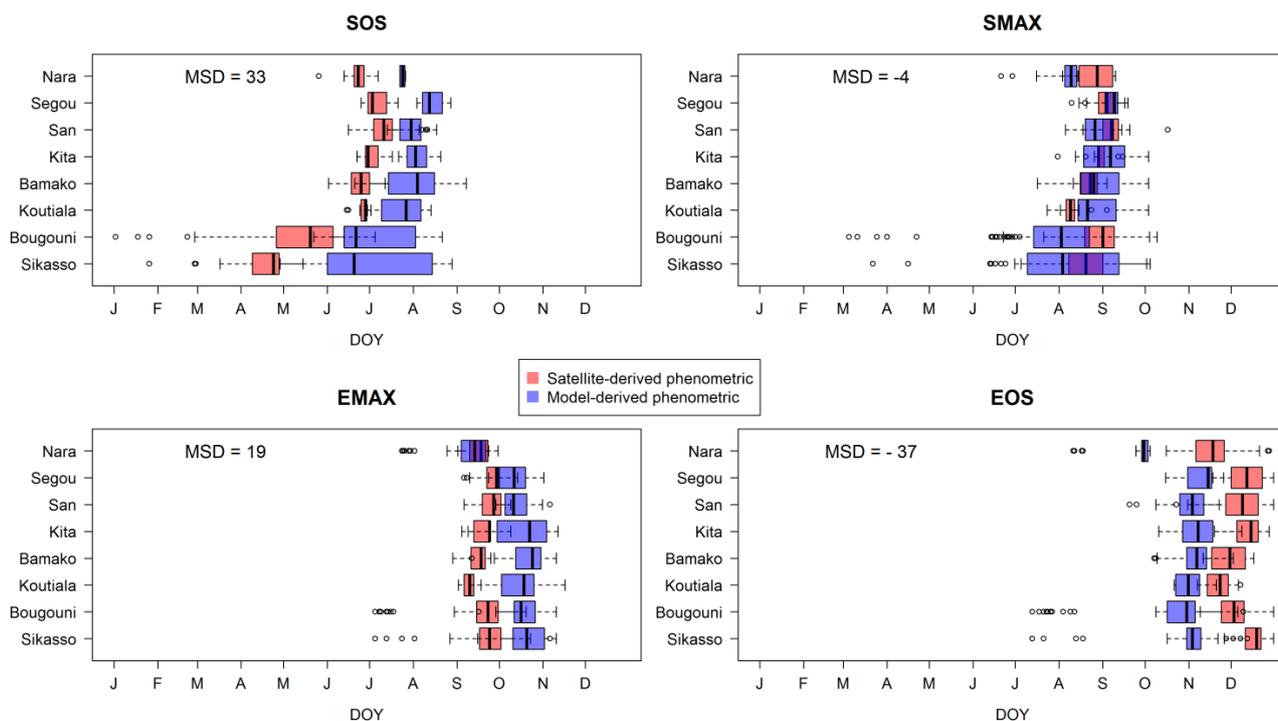
For the model- and satellite-derived phenometrics value variability in the 10 km × 10 km window around the stations, the SOS and SMAX distributions were wider for the Sudano-Guinean stations in Bougouni and Sikasso (standard deviation between 25 and 35 days) than for the other stations in the Sudanese and Sahelian regions (standard deviation between two and 20 days for SOS). For the satellite-derived phenometrics, the variability is that of the area taken around each station (20 × 20 pixels),

whereas for the model-derived phenometrics, the variability is due to the number of simulations performed for each station (Table 3).

The satellite-derived SOS and EMAX were detected before the model-derived phenometrics (MSD of 33 and 19 days, respectively), whereas the satellite-derived SMAX and EOS were detected after (MSD of -4 and -37 days, respectively).

4.2.2. A Comparison of the Satellite- and Model-Derived Phenometrics

The satellite- and model-derived phenometrics of the eight stations for 2007 were regressed against each other and compared. Figure 6 shows that the relationships between the satellite- and model-derived SOS, SMAX, and EOS are consistent among the stations (coefficient of correlation of 0.92, 0.74, and 0.65, respectively; *p*-value < 0.05). The SOS phenometrics yielded the best results; in contrast, the results were unsatisfactory for EMAX, especially for the Nara station (Figure 6).

Figure 6 also shows the RMSE, which is between seven and 12 days according to the phenometric.

Figure 6. Linear regression for the median satellite- and model-derived phenometrics values for the eight stations during 2007. The diagonal dotted lines represent the 1:1 line.
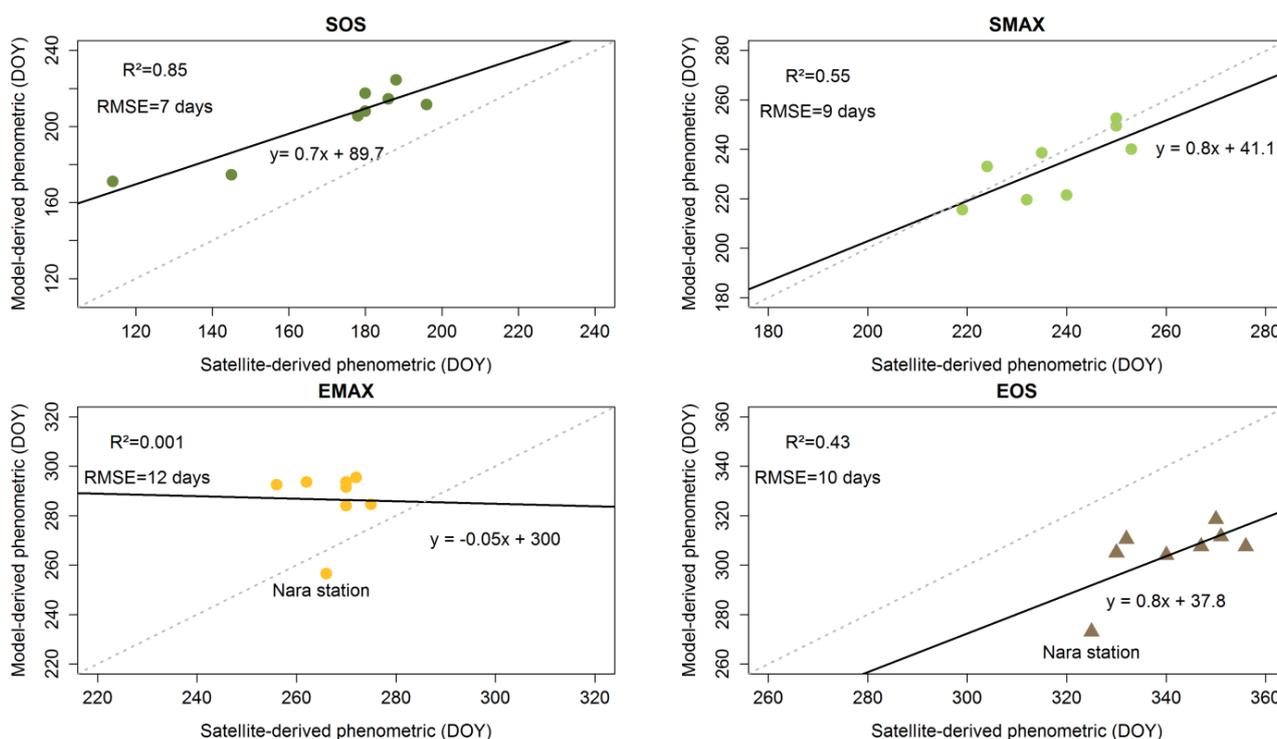
4.3. Phenometrics Temporal Analysis

4.3.1. Inter- and Intra-Annual Variations

Figure 7 shows the four MCD12Q2 product phenometrics calculated for Segou and Sikasso for 2002 to 2008 years.

For Segou, the year-to-year variation was slight for the four phenometrics, with a range of values of 11, 13, 6, and 8 days for SOS, SMAX, EMAX, and EOS, respectively. The intra-annual variation is

small too with a standard deviation comprised between five and 16 days according the years, as indicated by the short whiskers in Figure 7.

For Sikasso station, the inter-annual range of values is equivalent to that for Segou (23, 5, 5, and 4 days for SOS, SMAX, EMAX, and EOS, respectively). However, the intra-annual variations are particularly large for Sikasso, particularly in 2004 and 2006, with a standard deviation comprised between nine and 71 days.

Globally, the model-derived phenometrics for the Segou and Sikasso stations from 2002 to 2008 (Figure 7) display similar inter- and annual variations compared to the satellite-derived ones. However for Sikasso, the boxplots and whiskers were larger for model-derived SOS and SMAX, and the 2004 and 2006 years do not appear as anomalous for the EMAX and EOS.

As for the spatial analysis, the satellite-derived SOS were detected before the model-derived phenometrics (MSD of 33 and 52 days for Segou and Sikasso, respectively), whereas the satellite-derived EOS were detected after (MSD of -31 and -42 days for Segou and Sikasso, respectively).

Figure 7. Satellite- (pink) and model-derived phenometrics boxplots (violet) calculated for Segou and Sikasso from 2002 to 2008. The mean signed difference (MSD) corresponds to the difference in days between the model- and satellite-derived phenometrics.
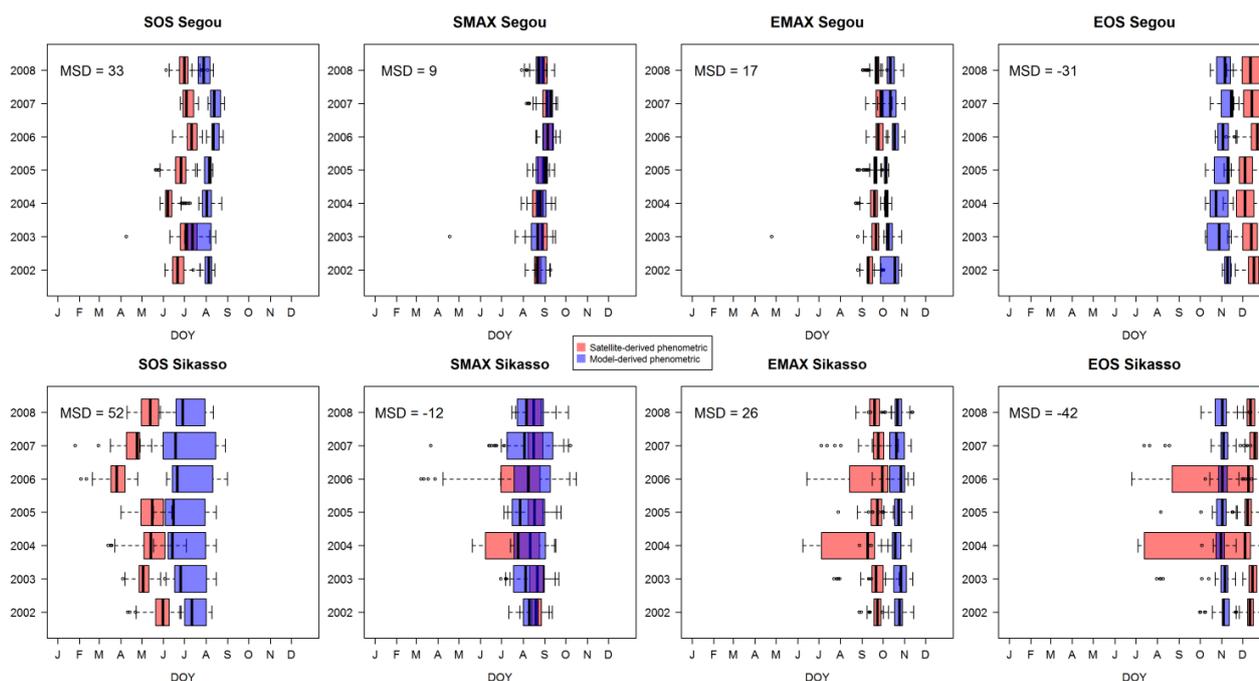

4.3.2. Comparison of the Satellite and Model-Derived Phenometrics

The satellite- and model-derived phenometrics for the years 2002 to 2008 were regressed against each other and compared for Segou and Sikasso stations. Figure 8 shows that the relationships between the satellite- and model-derived phenometrics are consistent, among the years, for Segou SMAX and EOS (coefficient of correlation of 0.68, and 0.70, respectively; *p*-value < 0.05), and that the satellite- and model-derived phenometrics are consistent among the years for Sikasso EMAX and EOS (coefficient of correlation of 0.7 and 0.65, respectively; *p*-value < 0.10). The inconsistency of Sikasso SOS phenometric was partly due to the year 2006 (orange point in Figure 8).

Figure 8 also shows the RMSE, which is between one and eight days according to the phenometric and the station.

Figure 8. Linear regression of the satellite- and model-derived phenometric median values for Segou and Sikasso from 2002 to 2008. The diagonal dotted lines represent the 1:1 lines. The SOS points represented by the orange circles were inconsistent for the rainfall distribution, which is discussed below (Section 4.4).
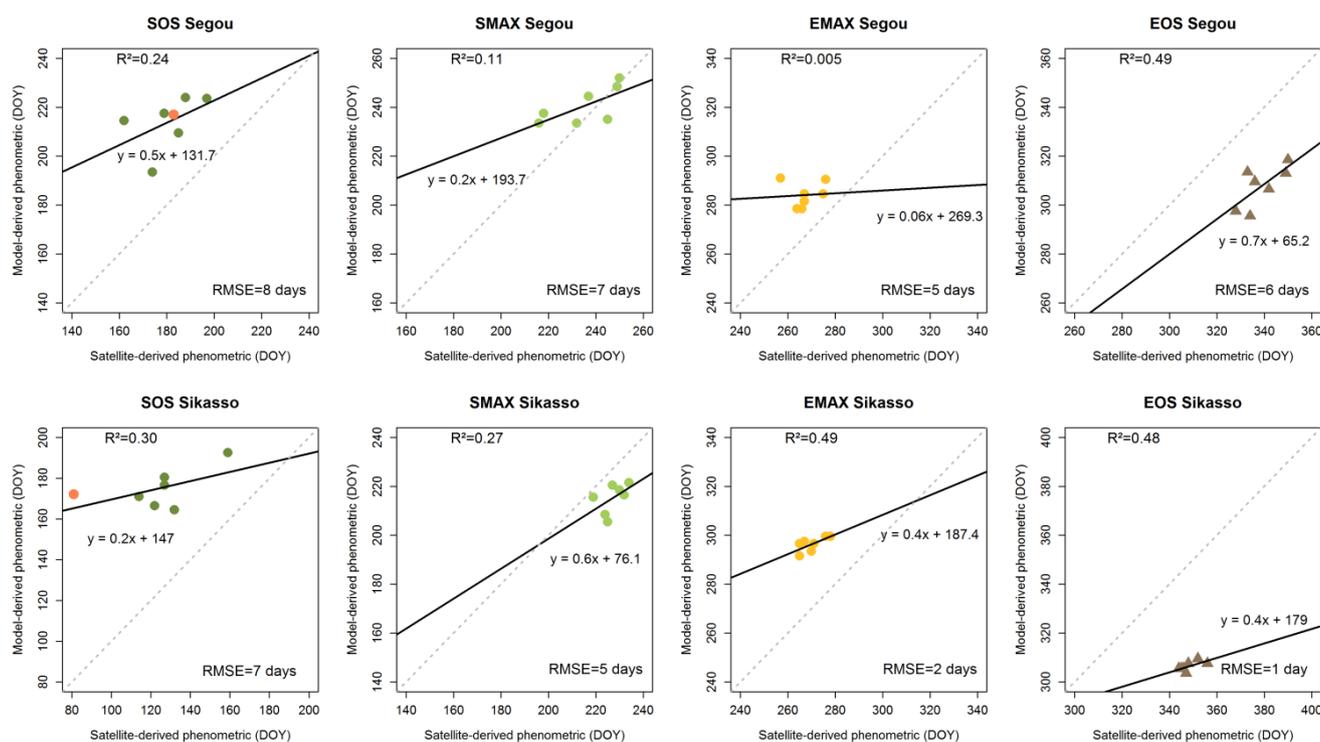

4.4. Inconsistencies Analysis

During the data analysis, we verified that the model- and satellite-derived start-of-season dates were consistent with the rainfall data. We observed certain inconsistencies, particularly in the SOS for Segou in 2002 (even if the point is not an outlier in the regression, see Figure 9) and Sikasso in 2006; the inconsistencies are further analyzed below.

- For Segou, in 2002, the time lag between the satellite- and model-derived phenometrics may be due to either satellite indices that were too early or model indices that were too late to detect the sowing dates. A closer look at the rainfall data showed that the satellite-derived SOS was consistent with the first rains. However, the model considered the rainfall levels and highlighted a false start in plant emergence, which is commonly referred to as failed sowing dates (Figure 9, with red circles that indicate failed sowing dates and green circles that indicate successful sowing dates). Thus, the model indicates that the plant was first sown on DOY 170 (such as for the satellite), but it did not grow properly and was re-sown 30 days later; this additional information from the model was not considered by the satellite.
- For Sikasso, in 2006, the satellite-derived SOS was detected two months before the first rains (Figure 9). The satellite-derived SOS was unusually early, and likely, the rain gauges may have

missed the first rains in the area, which raises questions on the spatial representativeness of the local rainfall measurements.

Figure 9. Rainfall (mm), LAI simulation (blue curve) and model- (dotted blue lines) and satellite-derived (dotted red lines) phenometric barplots for the two years, which indicate inconsistencies (Segou in 2002 and Sikasso in 2006), including for the LAI millet choho simulation in Segou and sorghum guinea in Sikasso (blue curve). From left to right, the dotted lines correspond to the start-of-season, start-of-maximum of season, end-of-maximum of season, and end-of-season, respectively. The red circle indicates a failed sowing date, and the green circle indicates a successful sowing date.
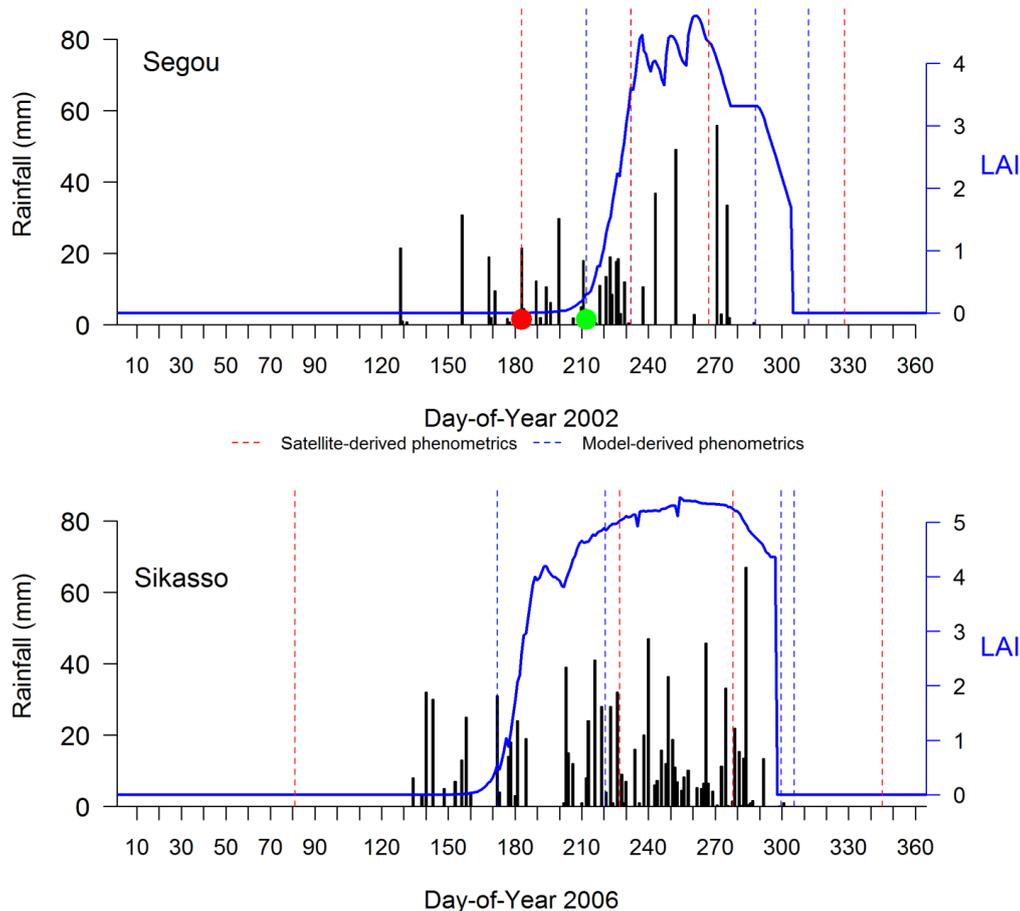
5. Discussions

5.1. Comparison between Satellite- and Model-Derived Phenometrics

First, the model- and satellite-derived phenometrics were separately analyzed for the eight stations in 2007; we observed that the season began sooner (May *vs.* July), with more variability for the start-of-season (SOS) and start-of-maximum of season (SMAX) (approximately 30 days *vs.* 10 days) in the south than in the north, except for Nara, wherein the season began early in 2007 (end of June). A similar crop calendar with related conclusions was also generated that highlighted the temporal (seven years) analyses for Segou and Sikasso. These results corroborate results from other studies [44,45]. The variability in the south, especially for the seedlings, was due to a greater variety of

species and varieties; cropping calendars must be adapted, not only to plant characteristics (species and photoperiod characteristics), but also to the beginning of the season [24]. The observation that satellite- and model-derived phenometrics in Sikasso vary more from year-to-year than in Segou, especially the SOS, suggests that natural vegetation is important in a humid site, wherein the transition dates may vary due to non-homogeneous land cover. This enhanced variability is also better reflected in the model that proposes various strategies based on expert knowledge, which is exemplified in the simulations through potential early sowing in the south, whereas only intermediary or late sowings were allowed in the north. Briefly, lower latitudes are consistent with longer rainy seasons and more choices by the farmers at the beginning of the crop season. For the end of the crop cycles, the two other phenometrics (EMAX and EOS) were concentrated in October and November, respectively, regardless of their location. The end of the rainy season was less variable than the beginning; farmer practice calendars are typically based on the average end of the rainy season [43].

Second, comparing satellite- and model-derived phenometrics for the stations in 2007, the satellite-derived SOS was approximately 30 days before the model-derived SOS. As vegetation and land cover are rarely uniform across 25 ha (500 m^2), the indications from the remotely sensed phenological indicators at the spatial resolution are unclear [28]. We hypothesized that the SOS delay may be due to a mix of the natural vegetation and crops in a pixel; natural vegetation begins at the beginning of the rainy season, while farmers typically wait for a certain level of rain before sowing [39]. Thus, the model-derived SMAX was earlier than the satellite-derived SMAX (four days), while the opposite was observed for the EMAX phenometrics (19 days). We assumed that the LAI profile simulations suggest that the cultivated patch was homogeneous with simultaneous growth for each plant, whereas the MODIS product inherently included a mix of land cover types. The LAI curve that represents pure crop phenology shows a curvature change before the MODIS mixed pixel; thus, the SMAX was earlier for the model. The EOS phenometrics difference was approximately 40 days for the model simulations and satellite observations. On the ground, the EOS approximately corresponds to the harvesting period, although the external environmental and socio-economic conditions may also play a role. For example, the harvesting date can either be sooner to avoid moisture for too much rain or immediate consumption, but it may be later due to a small working force or if the farmer practices allow the grains to dry up; these considerations may explain the later EOS detection using the satellite approach, typically 40 days after the model-derived EOS.

Comparing phenometrics from 2002 to 2008 in Segou and Sikasso, the RMSE remained approximately from one to eight days for the four phenometrics (*vs.* seven to 12 days for the eight stations in 2007), and the mean signed difference remained globally stable among the different climate conditions. The difference between the Segou and Sikasso metrics was approximately 30 days (50 days for Sikasso) for the model and satellite SOS images; the difference was 10 days for the SMAX, 20 days for the EMAX and 40 days for the EOS. Several sources of uncertainty in both the satellite and modeled data explain these differences.

5.2. Uncertainties, Data Limitations, and Interpretations

For the MCD12Q2 product, we showed in a previous study that the Zhang algorithm is not applicable in instances with greater than two consecutive missing 16-day NBAR EVI values, which is often the case in tropical West African countries [34]. Thus, artifacts can be introduced into the MODIS Land Cover Dynamics product due to the few opportunities for a clear view of the ground during the rainy season; thus, the data tend to be contaminated with clouds. Accurate results require good cloud screening and removing aerosols from the image. As a result, determining the SMAX and EMAX indicators from the MODIS Land Cover dynamics products was more difficult than determining the SOS and EOS, and we agree with Brown and de Beurs [20], who hypothesized that the different phenometrics performances (especially at the season maximum) would decrease due to cloud residue in the composite data. Thus, several cautions should be considered when using these phenological indicators. Our results are also consistent with [12], which showed that the MODIS NDVI composite data accurately predict phenology if the NDVI observations are not contaminated by clouds and are well-distributed over the main transition phases.

Second, the spatial resolution of this MODIS product (500 m) and the fact that we considered the main type of agricultural system (mixing two or three species in different proportions) at each station are also sources of inaccuracy [34]. At the pixel scale, the uncertainty is due to a mix of different land cover types in a pixel. At the station scale, we use various combinations of crop varieties, practices and soils based on geographic areas and expert knowledge to represent the variability of the situations. However, the model was not calibrated to force using the most suitable varieties for each area. In addition, although real field combinations can vary greatly, we did not weight the different simulations to avoid introducing more subjectivity and uncertainty.

Third, we observed certain inconsistencies with the rainfall data. The representativeness of the local rainfall information is questionable due to the convective rainfall regime; it is possible that a rainfall event (sporadic rain) may not be considered by the rain gauge in the two studied areas given the large spatial variability at a comparable site in Niger [17]. Thus, analyzing the representativeness of the variability observed from the satellite phenometrics would require a denser network, such as in Benin and in Niger, to study the utility of additional information from weather satellites for crop model results [46].

Despite the differences between the satellite- and model-derived transition dates, they are clearly related. The model-derived phenological indicators clearly simplify the ideal crop growth, whereas the satellite indicators are aggregated at 500 m and encompass several types of land cover. However, the differences are consistent, and spatial and temporal comparisons (with RMSEs at approximately five and nine days) suggest that the land cover dynamics derived from the MODIS time series can reproduce the spatial and temporal variability of different crop species and integrate both rainfall variability and land cover diversity. Our results are consistent with Xiao *et al.* [47], wherein large plains in North China and wheat/maize rotation systems were studied.

5.3. Crop Monitoring and Early Warning Systems

In Mali, it has been shown that except for the humid sub-region with dense cloud cover over more than 15 days, phenological indicators from the MCD12Q2 product are consistent with ground knowledge and modeling. However, in the food security context, the MCD12Q2 product cannot

be used because it is generally delivered the next year (MCD12Q2 is produced once a year from 24 months of input data, *i.e.*, including data for the 12 months of interest bracketed by six months of earlier and later data; see [30] for details). Zhang's algorithm [23] could also be used for the EVI time series during the growing season, and we observed that in the middle of the growing season, the algorithm can calculate the first two EVI curvature-change rates (*i.e.*, the SOS and SMAX for the season) [34]. As satellite observations are often contaminated by clouds during the maximum of the season in West Africa, this study mainly indicates that the observed SOS can easily be used in early warning systems for crop monitoring. For example, in semi-arid monsoonal ecosystems, where food crops are often photoperiodic, a sowing delay reduces the yield due to growing season length [48]. Therefore, combined with historical sowing date data, the satellite-derived SOS from the MODIS MCD12Q2 product could be used as an early warning indicator of risky conditions in the region. These data support a previous study from Brown and de Beurs [20], wherein existing methods that use sowing date ground observations were assessed, and the same SOS metric derived from multiple sensors and rainfall data was compared; a metric based on NDVI and relative humidity was developed therefrom. The linear regression between the observed sowing dates and MODIS eight-day composite with an 8-km spatial resolution showed a RMSE of approximately 12 days [20]. In addition, our outlier analysis suggested that the model and observations are complementary; they each provide different information. These observations reinforce our conviction that our method is relevant in countries where ground observations are scarce or difficult to collect; the combined use of satellite- and model-derived indicators of crop phenology should improve agricultural production estimates on a national scale in West Africa.

6. Conclusions

This paper documents the simultaneous use of remotely sensed indicators and a crop growth model to provide a better estimate of vegetation phenological changes in the data-scarce West African countries with food insecurity and a monsoonal ecosystem. We observed that the phenological indicators from the MODIS Land Cover Dynamics Yearly (MCD12Q2) product reproduce the spatio-temporal variability of crop phenological stages in Southern Mali.

Where the satellite observations are not contaminated by clouds and are well distributed over the transition phase, the start-of-season indicator could be recalculated from the EVI time series and used as complementary information with the crop model. Food security systems could benefit from such remotely sensed indicators, which provide spatially continuous information and vegetation phenological change information that integrates rainfall variability, land cover diversity, and farmer practices.

In the future, crop phenology monitoring should also benefit from ESA's upcoming satellite Sentinel-2, which will provide high spatial-, spectral- and temporal-resolution images of Earth on national and global scales.

Author Contributions

All authors contributed extensively to the work presented in this paper. Agnès Bégué, Christian Baron and Danny Lo Seen conceived and supervised the research topic. Elodie Vintrou and Agnès Bégué are the principal authors of this manuscript having written the majority of the manuscript and contributing at all phases of the investigation. Alexandre Saad performed the satellite datasets preprocessing. Christian Baron assisted with data analysis and provided expert knowledge about SARRA-H model. Danny Lo Seen participated in the methods selection and discussions but also in editing and revisions of the paper. Seydou Traoré provided rainfall dataset and contributed some portions of the written manuscript.

Conflicts of Interest

The authors declare no conflict of interest.

References

1. Becker-Reshef, I.; Justice, C.; Sullivan, M.; Vermote, E.; Tucker, C. Monitoring global croplands with coarse resolution earth observations: The global agriculture monitoring (GLAM) project. *Remote Sens.* **2010**, *2*, 1589–1609.
2. Sakamoto, T.; Yokozawa, M.; Toritani, H.; Shibayama, M.; Ishitsuka, N. A crop phenology detection method using time-series MODIS data. *Remote Sens. Environ.* **2005**, *96*, 366–374.
3. Zhang, X.; Friedl, M.A.; Schaaf, C.B.; Strahler, A.H.; Liu, Z. Monitoring the response of vegetation phenology to precipitation in Africa by coupling MODIS and TRMM instruments. *J. Geophys. Res. Atmos.* **2005**, *110*, doi:10.1029/2004JD005263.
4. Rembold, F.; Atzberger, C.; Savin, I.; Rojas, O. Using low resolution satellite imagery for yield prediction and yield anomaly detection. *Remote Sens.* **2013**, *5*, 1704–1733.
5. Kathuroju, N.; White, M.A.; Symanzik, J.; Schwartz, M.D.; Powell, J.A. On the use of the advanced very high resolution radiometer for development of prognostic land surface phenology models. *Ecol. Model.* **2007**, *201*, 144–156.
6. Reed, B.C.; Brown, J.F.; VanderZee, D.; Loveland, T.R.; Merchant, J.W. Measuring phenological variability from satellite imagery. *J. Veg. Sci.* **1994**, *5*, 703–714.
7. Zhang, X.; Friedl, M.; Schaaf, C. Sensitivity of vegetation phenology detection to the temporal resolution of satellite data. *Int. J. Remote Sens.* **2009**, *30*, 2061–2074.
8. Fritz, S.; Massart, M.; Savin, I.; Gallego, J.; Rembold, F. The use of modis data to derive acreage estimations for larger fields: A case study in the south-western rostov Region of Russia. *Int. J. Appl. Earth Obs. Geoinf.* **2008**, *10*, 453–466.
9. Atzberger, C. Advances in remote sensing of agriculture: Context description, existing operational monitoring systems and major information needs. *Remote Sens.* **2013**, *5*, 949–981.
10. White, M.A.; de Beurs, K.M.; Didan, K.; Inouye, D.W.; Richardson, A.D. Intercomparison, interpretation, and assessment of spring phenology in North America estimated from remote sensing for 1982–2006. *Glob. Chang. Biol.* **2009**, *15*, 2335–2359.

11. Schwartz, M.D.; Hanes, J.M. Intercomparing multiple measures of the onset of spring in Eastern North America. *Int. J. Climatol.* **2010**, *30*, 1614–1626.

12. Hmimina, G.; Dufrêne, E.; Pontailler, J.-Y.; Delpierre, N.; Aubinet, M. Evaluation of the potential of MODIS satellite data to predict vegetation phenology in different biomes: An investigation using ground-based NDVI measurements. *Remote Sens. Environ.* **2013**, *132*, 145–158.

13. Atkinson, P.M.; Jeganathan, C.; Dash, J.; Atzberger, C. Inter-comparison of four models for smoothing satellite sensor time-series data to estimate vegetation phenology. *Remote Sens. Environ.* **2012**, *123*, 400–417.

14. Funk, C.; Budde, M.E. Phenologically-tuned MODIS NDVI-based production anomaly estimates for Zimbabwe. *Remote Sens. Environ.* **2009**, *113*, 115–125.

15. Rojas, O.; Rembold, F.; Delincé, J.; Léo, O. Using the NDVI as auxiliary data for rapid quality assessment of rainfall estimates in Africa. *Int. J. Remote Sens.* **2011**, *32*, 3249–3265.

16. Atzberger, C.; Klisch, A.; Mattiuzzi, M.; Vuolo, F. Phenological metrics derived over the european continent from NDVI3G data and MODIS time series. *Remote Sens.* **2013**, *6*, 257–284.

17. Balme, M.; Galle, S.; Lebel, T. Démarrage de la saison des pluies au sahel: Variabilité aux échelles hydrologique et agronomique, analysée à partir des données epsat-Niger. *Sécheresse* **2005**, *16*, 15–22.

18. Heumann, B.W.; Seaquist, J.; Eklundh, L.; Jonsson, P. Avhrr derived phenological change in the Sahel and Soudan, Africa, 1982–2005. *Remote Sens. Environ.* **2007**, *108*, 385–392.

19. Wessels, K.; Steenkamp, K.; von Maltitz, G.; Archibald, S. Remotely sensed vegetation phenology for describing and predicting the biomes of South Africa. *Appl. Veg. Sci.* **2010**, *14*, 49–66.

20. Brown, M.E.; de Beurs, K.M. Evaluation of multi-sensor semi-arid crop season parameters based on NDVI and rainfall. *Remote Sens. Environ.* **2008**, *112*, 2261–2271.

21. Baron, C.; Sultan, B.; Balme, M.; Sarr, B.; Traoré, S.B. From GCM grid cell to agricultural plot: Scale issues affecting modelling of climate impact. *Philos. Trans. R. Soc. B: Biol. Sci.* **2005**, *360*, 2095–2108.

22. Oettli, P.; Sultan, B.; Baron, C.; Vrac, M. Are regional climate models relevant for crop yield prediction in West Africa? *Environ. Res. Lett.* **2011**, *6*, doi:10.1088/1748-9326/6/1/014008.

23. Zhang, X.; Friedl, M.A.; Schaaf, C.B.; Strahler, A.H.; Hodges, J.C.F. Monitoring vegetation phenology using modis. *Remote Sens. Environ.* **2003**, *84*, 471–475.

24. Traoré, S.B.; Alhassane, A.; Muller, B.; Kouressy, M.; Somé, L. Characterizing and modeling the diversity of cropping situations under climatic constraints in west africa. *Atmos. Sci. Lett.* **2011**, *12*, 89–95.

25. Kouressy, M.; Dingkuhn, M.; Vaksmann, M.; Heinemann, A.B. Adaptation to diverse semi-arid environments of sorghum genotypes having different plant type and sensitivity to photoperiod. *Agric. For. Meteorol.* **2008**, *148*, 357–371.

26. Soumare, M.; Bazile, D.; Vaksmann, M.; Kouressy, M.; Diallo, K. Agroecosystemic diversity and future of traditional cereals in the Malian cotton belt. *Divers. Agroecosystemique Devenir Cereales Tradit. Sud Mali* **2008**, *17*, 79–85.

27. Vintrou, E.; Soumaré, M.; Bernard, S.; Bégué, A.; Baron, C. Mapping fragmented agricultural systems in the Sudano-Sahelian environments of Africa using random forest and ensemble metrics of coarse resolution MODIS imagery. *Photogramm. Eng. Remote Sens.* **2012**, *78*, 839–848.

28. Zhang, X.; Friedl, M.A.; Schaaf, C.B. Global vegetation phenology from moderate resolution imaging spectroradiometer (MODIS): Evaluation of global patterns and comparison with *in situ* measurements. *J. Geophys. Res* **2006**, *111*, doi:10.1029/2006JG000217.

29. Ganguly, S.; Friedl, M.A.; Tan, B.; Zhang, X.; Verma, M. Land surface phenology from MODIS: Characterization of the collection five global land cover dynamics product. *Remote Sens. Environ.* **2010**, *114*, 1805–1816.

30. LP DAAC. Land Cover Dynamics Yearly l3 Global 500 m SIN Grid. Available online: https://lpdaac.usgs.gov/products/modis_products_table/mcd12q2 (accessed on 15 March 2012).

31. Huete, A.; Didan, K.; Miura, T.; Rodriguez, E.P.; Gao, X. Overview of the radiometric and biophysical performance of the MODIS vegetation indices. *Remote Sens. Environ.* **2002**, *83*, 195–213.

32. Beck, P.S.; Atzberger, C.; Høgda, K.A.; Johansen, B.; Skidmore, A.K. Improved monitoring of vegetation dynamics at very high latitudes: A new method using MODIS NDVI. *Remote Sens. Environ.* **2006**, *100*, 321–334.

33. Maatoug, L.; Arvor, D.; Simoes, M.; Bégué, A. Monitoring Crop Phenology in Mato Grosso (Brazil) Using Remote Sensing Data. In Proceedings of the 15th Sociedad Especialistas Latino-Americana en PErcepción Remota (SELPER) Symposium, French Guiana, France, 19–23 November 2012.

34. Vintrou, E.; Bégué, A.; Baron, C.; Lo Seen, D.; Saad, A. Analysis MODIS Phenometrics Quality on Cropped Land in West Africa. In Proceedings of the ESA Sentinel-2 Preparatory Symposium, Frascati, Italy, 23–27 April 2012.

35. Vintrou, E.; Desbrosse, A.; Bégué, A.; Traoré, S.B.; Baron, C. Crop area mapping in West Africa using landscape stratification of MODIS time series and comparison with existing global land products. *Int. J. Appl. Earth Obs. Geoinf.* **2012**, *14*, 83–93.

36. Dingkuhn, M.; Baron, C.; Bonnal, V.; Maraux, F.; Sarr, B. Decision Support Tools for Rainfed Crops in the Sahel at the Plot and Regional Scales. In *A Practical Guide to Decision-Support Tools for Agricultural Productivity and Soil Fertility Enhancement in Sub-Saharan Africa, IFDC, CTA*; Struif-Bontkes, T.E., Wopereis, M.C.S., Eds.; International Fertilizer Development Center: Muscle Shoals, AL, USA, 2003; pp. 127–139.

37. Baron, C.; Clopes, A.; Perez, P.; Muller, B.; Maraux, F. *Users Manuals for the: Sarramet (45 p.), Sarrabil (35 p.) and Sarrazon (29 p.) Softwares*; CIRAD: Montpellier, France, 1996.

38. Sultan, B.; Baron, C.; Dingkuhn, M.; Sarr, B.; Janicot, S. Agricultural impacts of large-scale variability of the West African monsoon. *Agric. For. Meteorol.* **2005**, *128*, 93–110.

39. Marteau, R.; Sultan, B.; Moron, V.; Alhassane, A.; Baron, C. The onset of the rainy season and farmers' sowing strategy for pearl millet cultivation in Southwest Niger. *Agric. For. Meteorol.* **2011**, *151*, 1356–1369.

40. Dingkuhn, M.; Kouressy, M.; Vaksmann, M.; Clerget, B.; Chantereau, J. A model of sorghum photoperiodism using the concept of threshold-lowering during prolonged appetence. *Eur. J. Agron* **2008**, *28*, 74–89.

41. Prince, S.D.; Goward, S.N. Global primary production: A remote sensing approach. *J. Biogeogr.* **1995**, *22*, 815–835.

42. *Advances in Integrated Soil Fertility Management in Sub Saharan Africa: Challenges and Opportunities*; Bationo, A., Waswa, B., Kihara, J., Kimetu, J, Eds; Springer: Berlin, Germany, 2007.

43. Kouressy, M.; Traoré, S.B.; Vaksmann, M.; Grum, M.; Maikano, I. Adaptation of Malian sorghums to climate variability. *Cah. Agric.* **2008**, *17*, 95–100.

44. Sultan, B.; Janicot, S.; Diedhiou, A. The West African monsoon dynamics. Part I: Documentation of intraseasonal variability. *J. Clim.* **2003**, *16*, 3389–3406.

45. Sultan, B.; Janicot, S.; Diedhiou, A. The West African monsoon dynamics. Part II: The "Preonset" and the "Onset" of the summer monsoon. *J. Clim.* **2003**, *16*, 3407–3427.

46. Ramarohetra, J.; Sultan, B.; Baron, C.; Gaiser, T.; Gosset, M. How satellite rainfall estimate errors may impact rainfed cereal yield simulation in West Africa. *Agric. For. Meteorol.* **2013**, *180*, 118–131.

47. Xiao, W.; Sun, Z.; Wang, Q.; Yang, Y. Evaluating MODIS phenology product for rotating croplands through ground observations. *J. Appl. Remote Sens.* **2013**, *7*, doi:10.1117/1.JRS.7.073562.

48. Buerkert, A.; Moser, M.; Kumar, A.K.; Fuerst, P.; Becker, K. Variation in grain quality of pearl millet from Sahelian West Africa. *Field Crop. Res.* **2001**, *69*, 1–11.